Numerical Simulation of Flute Modes in the GAMMA10 A-divertor

I.Katanuma, S.Masaki, S.Sato, K.Sekiya, M.Ichimura, and T.Imai

Plasma Research Center, University of Tsukuba, 1-1-1 Tennoudai, Tsukuba, Ibaraki 305-8577, Japan

The GAMMA10 tandem mirror is planning to install an axisymmetric divertor cell in it. Fig.1(a) is the GAMMA10, and Fig.1(b) is the present design of the GAMMA10 A-divertor, where the divertor/dipole region of GAMMA10 A-divertor is plotted in Fig.1(c).

There is a divertor plate, the shape of which is tentative, in the dipole region in Fig.1(c). All ions diffused radially in the central cell move along the separatrix (a magnetic flux tube, the field lines on which pass through the magnetic null [x-point]); those ions escape into a dipole region and then hit the divertor plate. The divertor simulation experiments of a large tokamak or a large helical device are expected to be realized in the GAMMA10 A-divertor.

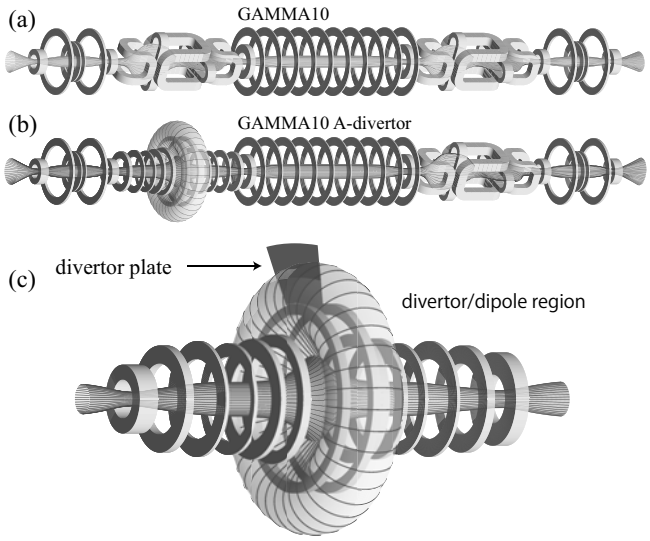

Figure 1: (a) GAMMA10, (b) GAMMA10 A-divertor and (c) divertor/dipole region with divertor plate

By the way, the most dangerous instability in the open magnetic system such as GAMMA10 is a flute instability. The GAMMA10 A-divertor is planning to stabilize the flute modes in the core region by a remaining anchor mirror cell and in the peripheral region by means of plasma compressibility[1], The divertor mirror cell, however, contains x-point, so a large plasma diffusion around the x-point breaks the stability condition [$\delta(pU^{\gamma})\delta U \geq 0$], which can make flute modes unstable, where p the plasma pressure, U the specific volume of a magnetic field line, δ means the variation in the outward direction.

The short circuit effects due to electrons on the separatrix is expected to stabilize the charge separation resulting from the centrifugal drifts there. Thus we have calculated the flute instabilities and its associated radial transport inside the separatrix with the boundary condition that the perturbed electrostatic potential $\widetilde{\phi} = 0$ on the separatrix[2,3]. The electric resistivity generated by the electron chaotic motion around x-point, however, may disturb the short circuit of electrons[4]. We, therefore, calculate the flute instability in the region including divertor and dipole regions of GAMMA10 A-divertor. Here, we do not assume the electron short circuit

around x-point.

We perform the computer simulation on the flute instabilities in the GAMMA10 A-divertor. The basic equations used here are the reduced MHD equations, which are described in Ref.[5]. In order to apply the equations, which were obtained in the assumption of the axisymmetric magnetic system, we revised the magnetic specific volume U as

$$U = \int \frac{\hat{p}_{\parallel}(\chi) + \hat{p}_{\perp}(\chi)}{B^2} \mathrm{d}\chi \tag{1}$$

Here pressures $p_{\parallel,\perp}$ are represented by a separation of variables $p_{\parallel,\perp}(\psi,\chi) = \hat{p}_{\parallel,\perp}(\chi)\nu(\psi)$. The coordinates (ψ,θ,χ), where the magnetic field B is described as $B = \nabla\psi \times \nabla\theta = \nabla\chi$, are adopted.

The flute stability condition $[\delta(pU^{\gamma})\delta U \geq 0]$ is written in terms of U in Eq.(1)[2,3],

$$\partial U/\partial\psi \leq 0 \tag{2}$$

in the case that the compressional term $pU^{\gamma-1}(\delta U)^2$ is neglected compared to $U^{\gamma}\delta p\delta U$, which is used to flute mode stability analysis in a long thin magnetic field, because the relation $\delta p \leq 0$ is satisfied in the experimental devices. Equation (2) means that the flute modes are stabilized by the good magnetic field line curvature.

Fig.2 illustrates the axial pressure profiles in the GAMMA10 A-divertor, where the pressure in the anchor mirror cell ($z \simeq -520$cm) is taken to be higher than that in other cells in order to stabilize the flute modes in the core region.

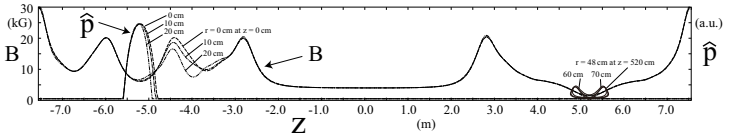

Figure 2: Axial pressure profiles $\hat{p} = \hat{p}_{\parallel}(\chi) + \hat{p}_{\perp}(\chi)$ in GAMMA10 A-divertor.

The specific volume is plotted in Fig.3 for various p_A, where p_A is the ratio of anchor pressure to the central cell pressure. Here $x \equiv \sqrt{\psi/\psi_b}$, where ψ_b is the coordinate of the boundary in the dipole region. The separatrix is located at $x = x_{null} \simeq 0.63$. The case $p_A = 1$ shows that $\partial U/\partial x > 0$ inside x_{null}, which is unstable to the flute modes, while the case $p_A = 14$ shows that $\partial U/\partial x < 0$ inside $x \simeq 0.26$ and $\partial U/\partial x > 0$ in $0.26 < x < x_{null}$.

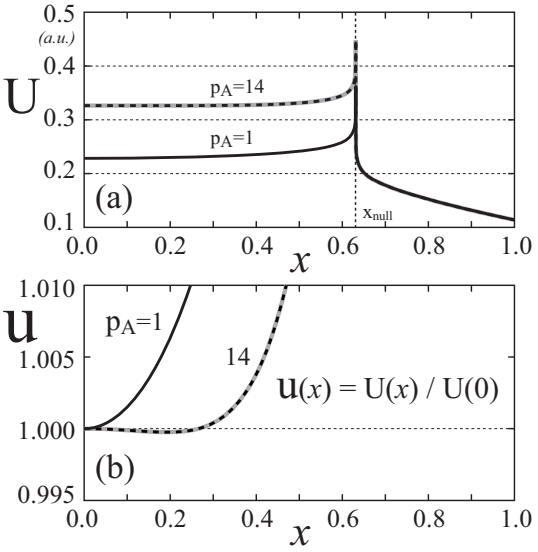

Figure 3: Specific volume of magnetic field line.

At the separatrix $U \to \infty$ due to $B \to 0$. But ions feel the average magnetic field during gyroperiod, so U is expected to have a finite value averaged over the ion gyromotion. The derivative $\partial U/\partial x < 0$ inside the dipole region means that the flute modes are stabile there.

At first the simulation results in case $p_A = 1$ are shown. Initial conditions are that $D_E(x,\theta) = 1.0$, $T_E(x,\theta) = 1.0$, $w_0(x,\theta) = 1.0$ in $x < x_{null}$ and $D_E(x,\theta) = 0.1$, $T_E(x,\theta) = 0.1$, $w_0(x,\theta) = 0.1$ in $x_{null} < x < 1$. Here $T_E(x,\theta) = T(x,\theta)U(x)^{2/3}$, $D_E(x,\theta) = \rho(x,\theta)U(x)$, where $T(x,\theta)$, $\rho(x,\theta)$ are plasma temperature and mass density, $w_0(x,\theta)$ $\left[\simeq \int (\mathrm{d}\chi/B^2)B\cdot\nabla\times(\rho v)\right]$ is the vorticity, details of which are described in Ref.[2, 3].

Fig.4 plots the time evolution of electrostatic potential observed at $x = 1/2$, where m is the azimuthal mode number of Fourier components. The dashed line is the growth rate calculated by the non-local linear analysis, where the radial profiles of D_E, T_E and w_0 at $\tau = 75$ were used in the analysis which is shown in Fig.5. Here τ is the normalized time. The flute instability grows through the linear phase and enters the nonlinear saturation phase, the phase of which continues with high amplitude in time.

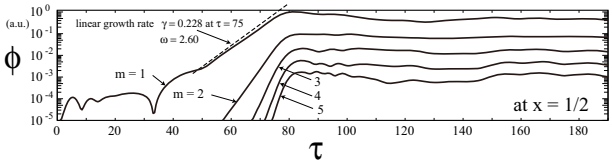

Figure 4: Time evolution of electrostatic potential $\widetilde{\phi}$ observed at $x = 1/2$ in case of $p_A = 1$. Here m is the azimuthal mode number.

Fig.5 plots the radial profiles averaged over θ at $\tau = 75$. The radial profiles of D_E and T_E around $x = x_{null}$ show the large radial transport around the separatrix (note that $D_E \propto U$ and $T_E \propto U^{2/3}$). Fig.5(c) is the radial profile of $m = 1$ Fourier amplitude of $\widetilde{\phi}$ observed in the simulation. The flute mode is found to be localized inside x_{null} and there is no flute instability outside x_{null} in Fig.5(c).

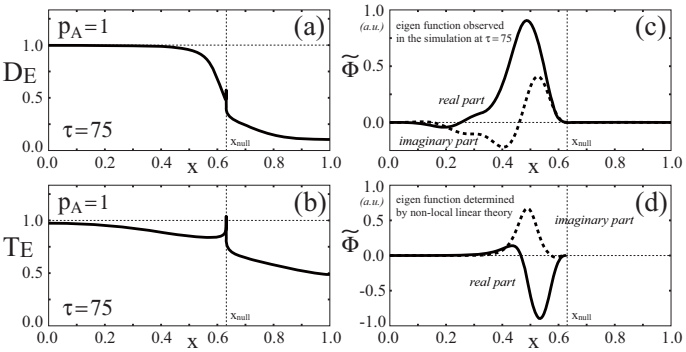

Figure 5: Radial profiles of (a) D_E, (b) T_E averaged over θ at $\tau = 75$, and (c) $m = 1$ electrostatic potential $\widetilde{\phi}$ in case of $p_A = 1$. (d) is the radial profile of $\widetilde{\phi}$ calculated by the nonlocal linear analysis.

The nonlocal linear analysis was carried out by using the radial profiles just mentioned above. The resultant eigen-function is plotted in Fig.5(d). The eigen-function were calculated from $x = 0$ with the boundary conditions but the solution was not determined beyond x_{null}, thus the eigen-function is not drawn beyond x_{null} in Fig.5(d).

The contours of D_f and T_f plotted in Fig.6 at $\tau = 80$ indicates that the flute mode perturbations are localized inside x_{null}. The flute fluctuations are quite

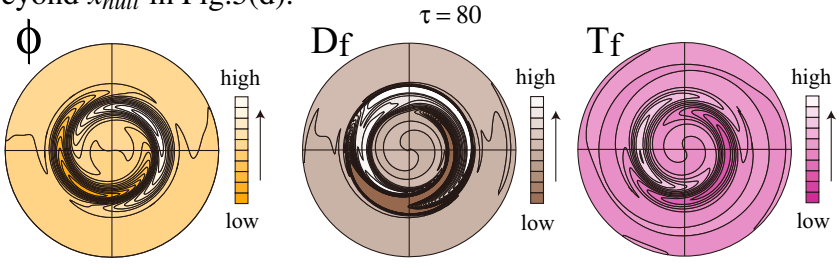

Figure 6: Contour plots of $D_f(x,\theta)$ and $T_f(x,\theta)$. Here D_f and T_f are the variables in which $m = 0$ component is eliminated from D_E and T_E.

small in the dipole region
(outside x_{null}), which is consistent with the results in Fig.5.

The case of $p_A = 14$ is plotted in Figs.7 and 8. Even that $\partial U/\partial\psi < 0$ near axis (where is stable to the flute modes), the flute is unstable as a whole and after the linear growing phase the flute instabilities enter the nonlinear saturation phase. The linear growth rate observed in the simulation agrees with that calculated by the nonlocal linear analysis by using the radial profiles of w_0, D_E and T_E observed in the simulation at $\tau = 90$. The flute mode fluctuations are kept high level in the nonlinear saturation state as in the case of $p_A = 1$.

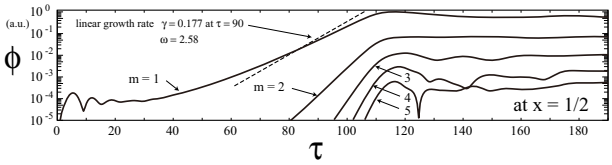

Figure 7: Time evolution of electrostatic potential $\widetilde{\phi}$ observed at $x = 1/2$ in case of $p_A = 14$. Here m is the azimuthal mode number.

The radial profiles of D_E and T_E averaged over θ in Figs.8(a) and 8(b) show the large diffusion around x_{null}. The flute instability has enhanced the radial transport of T_E in $0.2 \lesssim x \leq x_{null}$. The eigen-function of $\widetilde{\phi}$ is localized inside x_{null} in Fig.8(c). The eigen-function calculated by the nonlocal linear analysis Fig.8(d) agrees with that observed one in Fig.8(c).

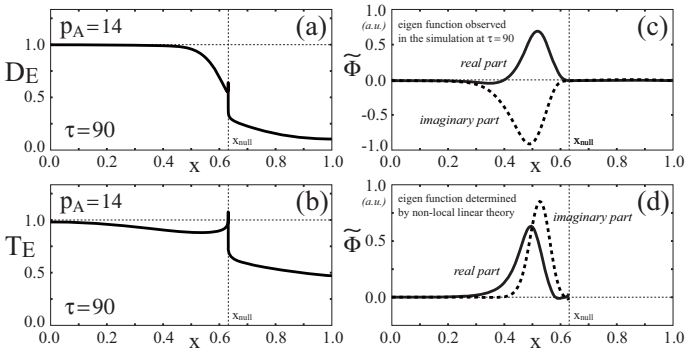

Figure 8: Radial profiles of (a) D_E, (b) T_E averaged over θ at $\tau = 75$, and (c) $m = 1$ electrostatic potential $\widetilde{\phi}$ in case of $p_A = 14$. (d) is the radial profile of $\widetilde{\phi}$ calculated by the linear analysis.

In summary we performed the simulations on the flute mode instabilities in the divertor/dipole region of the GAMMA10 A-divertor. We have calculated only in the divertor region with the boundary condition that the perturbation of ϕ is zero along the boundary (magnetic null) before[2,3]. So this paper is the first calculation including the dipole region as well as the divertor. The results of the simulation indicate that the magnetic null can suppress the flute mode fluctuations there even if the effects of electron short circuit is removed in the simulation.

[1] Y.Sasagawa, I.Katanuma, Y.Mizoguchi, T.Cho, V.P.Pastukhov, Phys. Plasmas, **13**, 122506 (2006).

[2] I.Katanuma, K.Yagi, Y.Nakashima, M.Ichimura, and T.Imai; Phys. Plasmas, **17**, 032303 (2010).

[3] I.Katanuma, K.Yagi, Y.Haraguchi, N.Ichioka, S.Masaki, M.Ichimura, and T.Imai; Phys. Plasmas, **17**, 112506 (2010).

[4] R.Numata and Z.Yoshida, Phys, Rev. Lett. **88**, 045003 (2002).

[5] V.P.Pastukhov, Fiz. Plazmy, **31**, 628 (2005) [Plasma Phys. Rep. **31**, 577 (2005)